Virchows Archiv (1994) 424:677–685

ORIGINAL ARTICLE

J. C. Papadimitriou · C. B. Drachenberg · M. L. Shin
B. F. Trump

Ultrastructural studies of complement mediated cell death: a biological reaction model to plasma membrane injury

Received: 29 June 1993 / Accepted: 24 March 1994

Abstract Complement-mediated nucleated cell death has been shown to be independent of colloid-osmotic swelling. In contrast, other factors (e.g. Ca^{2+} influx) are of importance in the induction of cell death. In this communication, the sequential morphological features of complement-mediated cell injury have been studied by electron microscopy and compared with biochemical data (ATP content and LDH release). It was observed that immediately after C5b–8 lesion formation, although the overall cell morphology is well preserved, the mitochondria display an "ultracondensed" appearance. Upon addition of C9, the mitochondria remain initially condensed, but swell progressively with final formation of flocculent densities. The nuclei become progressively edematous, with concurrent disappearance of heterochromatin. The nucleoli lose their associated chromatin and display segregation of their components with formation of markedly electron-dense filamentous deposits. The nuclear envelope remains initially intact, but subsequently progressive dilatation of the associated perinuclear RER cisterna and distention of the nuclear pores associated with leakage of chromatin into the cytoplasm are seen. The larger cell organelles (including mitochondria, ER, Golgi apparatus, etc.) become clustered around the nucleus, concurrently with marked edema of the outer cytoplasm and bleb formation. The RER cisternae become dilated, whereas the Golgi complex disappears. Relatively early on the plasma membrane shows breaks in continuity. The pattern of these changes – potentially related to Ca^{2+} influx, ATP efflux and overall metabolic depletion – corresponds to the previously described model of cell reaction to injury, confirming the dynamic nature of the process. The morphology of cell death in this model shares some features, e.g., the nucleolar changes, with "apoptosis" (programmed cell death). However, the overall pattern appears to correspond more to "necrosis," characterized by loss of volume control and mitochondrial abnormalities.

Key words Complement – Cell injury – Ehrlich Ascites cells – Cell death

Introduction

Cells can be injured among other factors through the action of xenobiotic chemicals, anoxia, and physical changes such as radiation and trauma (for review see Trump and Berezesky 1992). Reaction to cell injury is defined as "a state of pathologically altered cell function" (Marzella and Trump 1992) deviating from the normal homeostasis condition. Despite differences in the initial insult, injured cells may manifest common structural and functional alterations.

The ultrastructural and biochemical changes occurring in the cell following inhibition of ATP synthesis or interference with cell membrane function have been extensively studied in Ehrlich ascites tumor cells (EATC). Specifically, a series of mitochondrial changes (condensation or C phase, swelling or S phase, and accumulation of flocculent densities) has been clearly demonstrated in various forms of cell injury (Laiho and Trump 1975). These changes, together with other subcellular alterations, have led to the schematic separation of cell injury into sequential stages (Trump et al. 1980). This model has been well established following anoxia. Although the pattern of changes has been similar with cell membrane injury, the latter model has been tested only with the use of exogenous chemical agents, e.g., calcium ionophores, amphotericin B or PCMBS (Saladino et al. 1969; Laiho et al. 1971). The biological membrane channel formers, such as complement and lymphocyte-dependent killing factors, have not been examined in that context. Since the latter forms of injury correspond to major in vivo phenomena, including immunity against tumors, allo-

Contribution no. 3372 from the Cellular Pathobiology Laboratory

J.C. Papadimitriou (✉) · C.B. Drachenberg · M.L. Shin
B.F. Trump
University of Maryland School of Medicine, Department of Pathology, 10 South Pine Street, Baltimore, MD 21201, USA

B.F. Trump
Maryland Institute for Emergency Medical Services Systems, Baltimore, MD 21201, USA

graft rejection etc., their study is strongly indicated. Recently a great amount of data has been accumulated on the issue of apoptosis (programmed cell death). It has been proposed that whereas both cell-mediated cytotoxicity and calcium ionophores cause cell death by apoptosis, complement membrane attack leads to cell necrosis (for review see Schwartzman and Cidlowski 1993). These conclusions are based mainly on DNA degradation data. However, since apoptosis is to a significant extent morphologically defined, ultrastructural studies appear necessary for clarification of the issue. These observations will contribute towards a better understanding of the process of cell death and specifically the definition of the "point of no return", that is to say the point after which recovery is not possible and the cells are committed to dying (for review see Marzella and Trump 1992).

Materials and methods

Complement-mediated cell death occurs when the components C5 to C9 produce heteropolymeric (C5b–9) channels, which are inserted in the plasma membrane and thus disrupt the ionic and energy regulation of the cell. In order to analyze this process kinetically, the cells are first loaded with antibodies against their membranes and then exposed to serum containing all complement components except for C8 or C9. The latter component is necessary for the creation of large transmembrane channels (for review see Papadimitriou et al. 1990). Specifically, the following reagents were used. Veronal-buffered saline, pH 7.4 (145 mM NaCl, 5 mM sodium barbital) was prepared by diluting a stock solution 5fold with water (Kabat and Mayer 1961). GVB^{++} contained 0.1% gelatin, 0.15 mM $CaCl_2$, and 1.0 mM $MgCl_2$. $DGVB^{++}$ was veronal-buffered saline containing 5 mM sodium barbital, 72.5 mM NaCl, 2.5% dextrose, 0.1% gelatin, 0.15 mM $CaCl_2$ and 1.0 mM $MgCl_2$. DVB^{++} was identical to $DGVB^{++}$ except that the gelatin addition was omitted.

Polyclonal antisera against EATC were obtained by immunizing rabbits with cell membranes, and the IgG fraction was prepared as described (Carney et al. 1985). Human sera immunochemically depleted of C8 (C8D–HS) or C9 (C9D–HS) and purified human C8 and C9 were purchased from Quidell (LaJolla, Calif.).

EATC were grown in peritoneal cavities of mice by weekly transplantation. Harvested cells were washed in $DGVB^{++}$ by centrifugation at 200 *g* for 10 min at 4° C and were resuspended to 5× 10^6 cells/ml of $DGVB^{++}$. EATC carrying C5b–7 or C5b–8 were prepared as described previously (Carney et al. 1985). In brief, cells bearing the appropriate number of C5b–7 (TAC7) or C5b–8 complexes (TAC8) that would lead to 80% cell lysis after addition of C8+C9 or C9, respectively, were prepared by incubating antibody-sensitized tumor cells (TA) at 37° C for 15 min with an equal volume of diluted C8D–HS (1:40) or C9D–HS (1:60), respectively. The washed cells were kept on ice, at 2.5× 10^6 cells/ml of $DGVB^{++}$, until use. Cytotoxic assays and adenine nucleotide measurements were performed by incubating 100 µl of TAC7 with excess C8 plus C9, or 100 µl TAC8 cells with excess C9, at 37° C. At desired time points, cells were centrifuged at 3000 rpm for 1 min at 4° C. Cell pellets and supernatants were examined for the levels of adenine nucleotides. LDH was determined in the supernatant as an index of cell death (Koski et al. 1983).

ATP assays were performed by luminometry as described elsewhere (Thore 1979) in a 1250 LKB luminometer with reagents supplied by LKB-Wallace (Gaithersburg, Md.), with duplicate or triplicate samples. To measure adenine nucleotides in cells, the cell pellet was first extracted with 0.2 ml of 2% TCA in 1 mM EDTA for 10 min at 20° C. To determine AMP and ADP in cell pellets and supernatants, AMP and ADP were converted to ATP by incubating the samples with myokinase (25 µg/ml), phosphoenol pyruvate (1 mM), pyruvate kinase (25 µg/ml), and 5 µl/ml ATP (10 µM) (Sigma, St. Louis, Mo.) for 60 min at 20° C. The total ATP was then determined. The amounts of ADP and AMP were calculated by substracting the ATP values obtained from the preincubation sample from the total ATP. The results were expressed as absolute nmoles in a 0.5× 10^6 cell pellet or supernatant by using standard curves obtained in each assay.

The cell pellets, obtained at various time points, were immediately fixed in 0.6 ml of 2% glutaraldehyde (Sigma) in DVB^{++}, for 60 min at room temperature. Cells were washed three times in DVB^{++} and then suspended in 0.1 M sodium cacodylate buffer, pH 7.4, containing 0.2 M sucrose. Post-fixation with osmium was followed by en bloc staining with uranyl acetate before dehydration through graded alcohols and Epon embedding (Luft 1961). Ultrathin sections were stained with 0.5% uranyl acetate and 1% lead citrate (Watson 1958; Venable and Coggeshall 1965). Transmission electron microscopy was performed with a JEOL 100–B electron microscope. Morphologic changes of mitochondria were classified into three groups: orthodox (O), condensed (C), and swollen (S), according to the criteria described by Laiho and Trump (1975).

Results

The C5b–8 lesions were titrated by assessing their half-life. When excess C9 was added immediately, 80% of the cells were killed, in contrast to 37%, 21% and 18% when the C5b–8 lesion-bearing cells were preincubated in 37° C for 10, 20 or 30 min, respectively. This C5b–8 disappearance has previously been shown to be related to endocytosis of the lesions (Carney et al. 1985). With identical experimental conditions, we have previously studied these lesions immunochemically by fluorescence-activated cell scanning (FACS), showing persistence of 78%, 68% and 60% of the initial lesions (considered as 100%) after 10, 20, and 30 min incubation, respectively (Papadimitriou et al. 1991d).

Whereas no AMP or ADP was detected in the medium surrounding C5b–7-bearing cells, upon addition of C8 up to 0.1 nmol/0.5× 10^6 cells of AMP+ADP was leaked to the medium, reaching the peak level 20 min after the addition of C8. The cells remained viable (i.e., no LDH release was observed during the 60-min period of observation), and their intracellular ATP content did not decrease (see below).

In contrast to the C5b–8-bearing cells, the cell ATP content dropped to <20% within 30 s after the C5b–9 formation, whereas the LDH release – indicating cell lysis – first became appreciable at 5 min (Fig. 1).

These results are consistent with the studies performed by us on individual cells by digital imaging fluorescence microscopy (Papadimitriou et al. 1991a). In these studies, cell death was assessed with nuclear staining by propidium iodide. The kinetics of cell death were almost identical to the LDH release pattern.

The untreated EATC had a roughly spherical shape, with abundant *microvilli* and reniform, relatively convoluted *nuclei* (Fig. 2). The latter contained prominent round *nucleoli,* surrounded by nucleolus-associated chromatin (Fig. 2, insert). Within the nucleolus itself, pale-staining areas could be discerned, surrounded by rela-

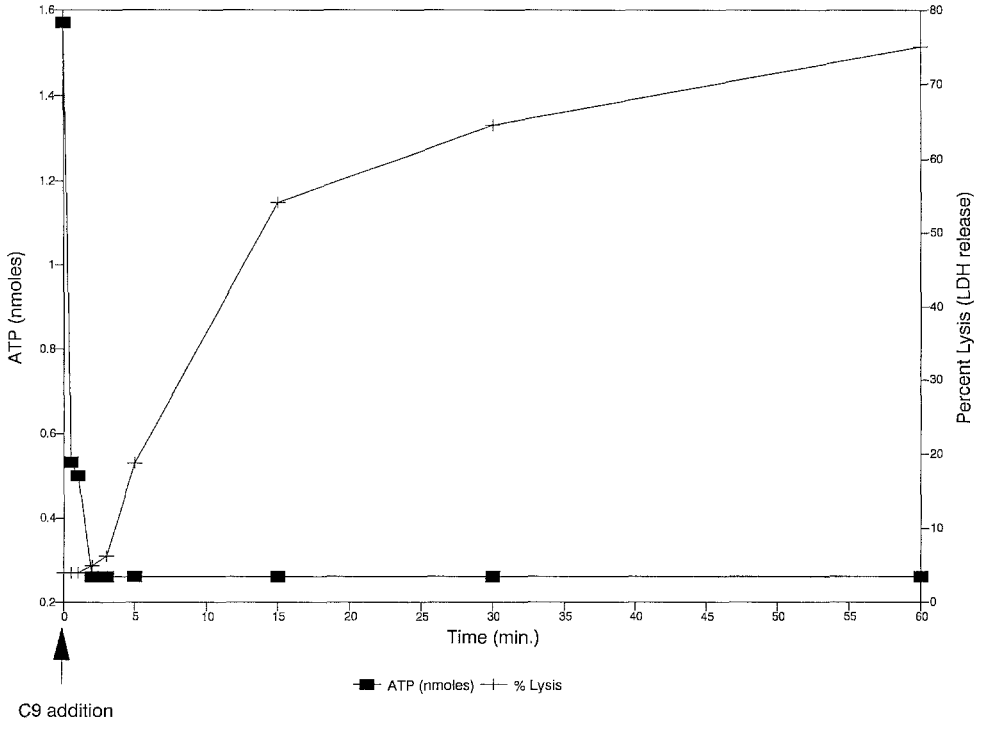

Fig. 1 Immediately (30 s) after C5b–9 lesion formation, the cell ATP drops to <20%. The LDH release – indicating cell lysis – first becomes appreciable at 5 min

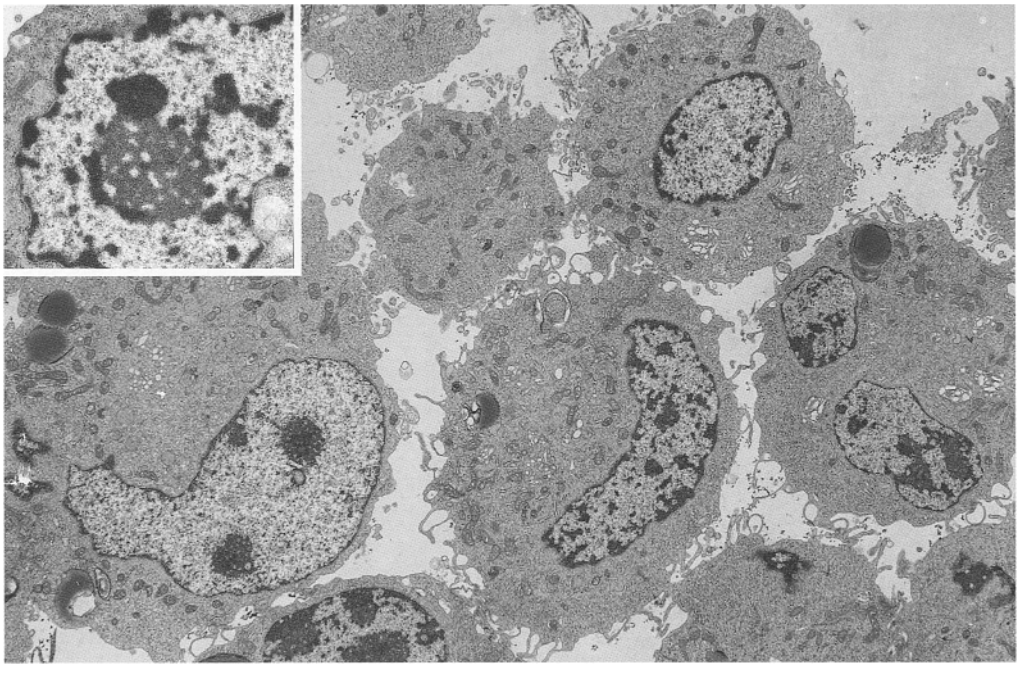

Fig. 2 Untreated Ehrlich Ascites tumor cells (EATC) are roughly spherical in shape, with prominent microvilli, evenly distributed organelles, and relatively convoluted nuclei. (× 5,300) The latter show prominent nucleoli with distinct components and associated heterochromatin (*insert,* × 10,600)

tively homogeneous nucleolonema. The distinction between fibrillar and granular component was prominent only in a portion of the cells.

The morphology of the *mitochondria* varied between orthodox (O) and condensed (C), depending on the temperature of the medium: At 0–4° C, they were mostly in the C-phase (Fig. 3B), whereas at 37° C the 0-morphology was almost universally assumed (Fig. 3A). In the latter morphological stage, the matrix displayed prominent electron-dense granules.

The *endoplasmic reticulum* cisternae were mostly non-dilated, whereas the Golgi complex was clearly discernible (Fig. 3B).

The *cytoskeletal* elements, including microtubules, actin, and intermediate filaments, as well as the various cytoplasmic organelles, were relatively evenly distributed (Fig. 2). The cytoplasm contained several lipid vacuoles (Fig. 2).

The TAC8 cells showed mild simplification of their surface, with most microvilli preserved though shorter

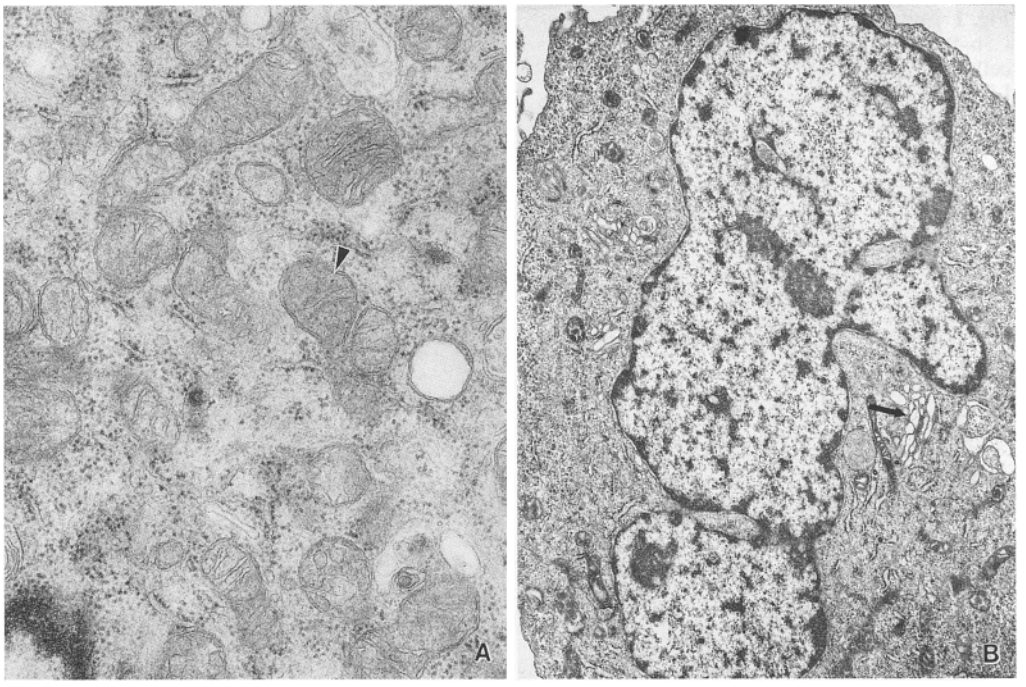

Fig. 3A The mitochondria display at 37° C an orthodox (0) morphology with distinct intracristal granules *(arrowhead)*. (× 32,000). **B** At 0° C, the mitochondria assume a condensed (C) morphology. The Golgi complex is prominent in untreated cells *(arrow)*. (× 11,000)

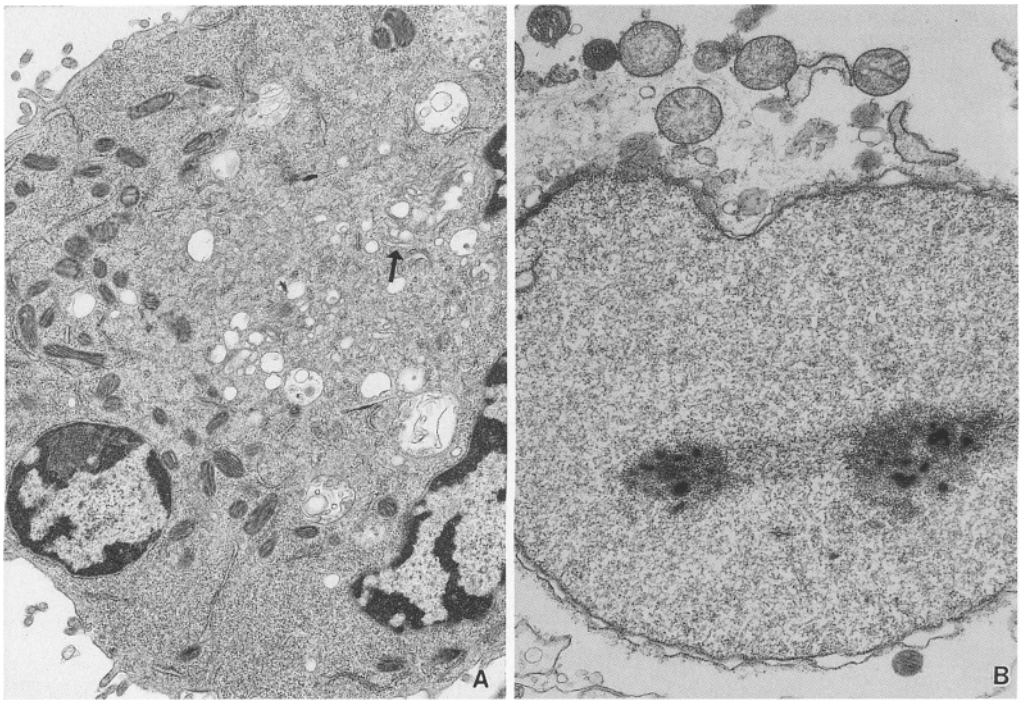

Fig. 4A At 37° C, for the first 30 min of incubation (here after 15 min), cells bearing C5b–8 lesions show ultracondensed mitochondria. The microvilli are mostly retained, and the Golgi complex is somewhat distorted but still discernible *(arrow)*. (13,300). **B** After 60 min, however, cells bearing C5b–8 lesions show segregation of the nucleolar components as well as mitochondrial swelling, although no LDH release is found in the supernatant (× 13,300)

and thicker. The nuclei were not swollen. The mitochondria remained in the C-phase for up to 30 min, irrespective of the temperature of the medium (i.e., at both 0–4° C and 37° C). The RER cisternae were not dilated, but the Golgi complex showed some disorganization. The organelles were homogeneously distributed throughout the cytoplasm (Fig. 4A). No significant changes from that morphological pattern were observed in TAC8 cells during the first 30 min of incubation at 37° C. Between 30 and 60 min of incubation, however, the mitochondria showed progressive swelling and the nucleus displayed heterochromatin dissolution and electron-dense nucleolar deposits. The cells did not appear swollen overall, however (Fig. 4B).

The TAC9 cells appeared at 0–4° C significantly swollen, with disappearance of most microvilli (Fig. 5A). All the larger organelles clustered around the nucleus, whereas the cytoplasm showed several early bleb for-

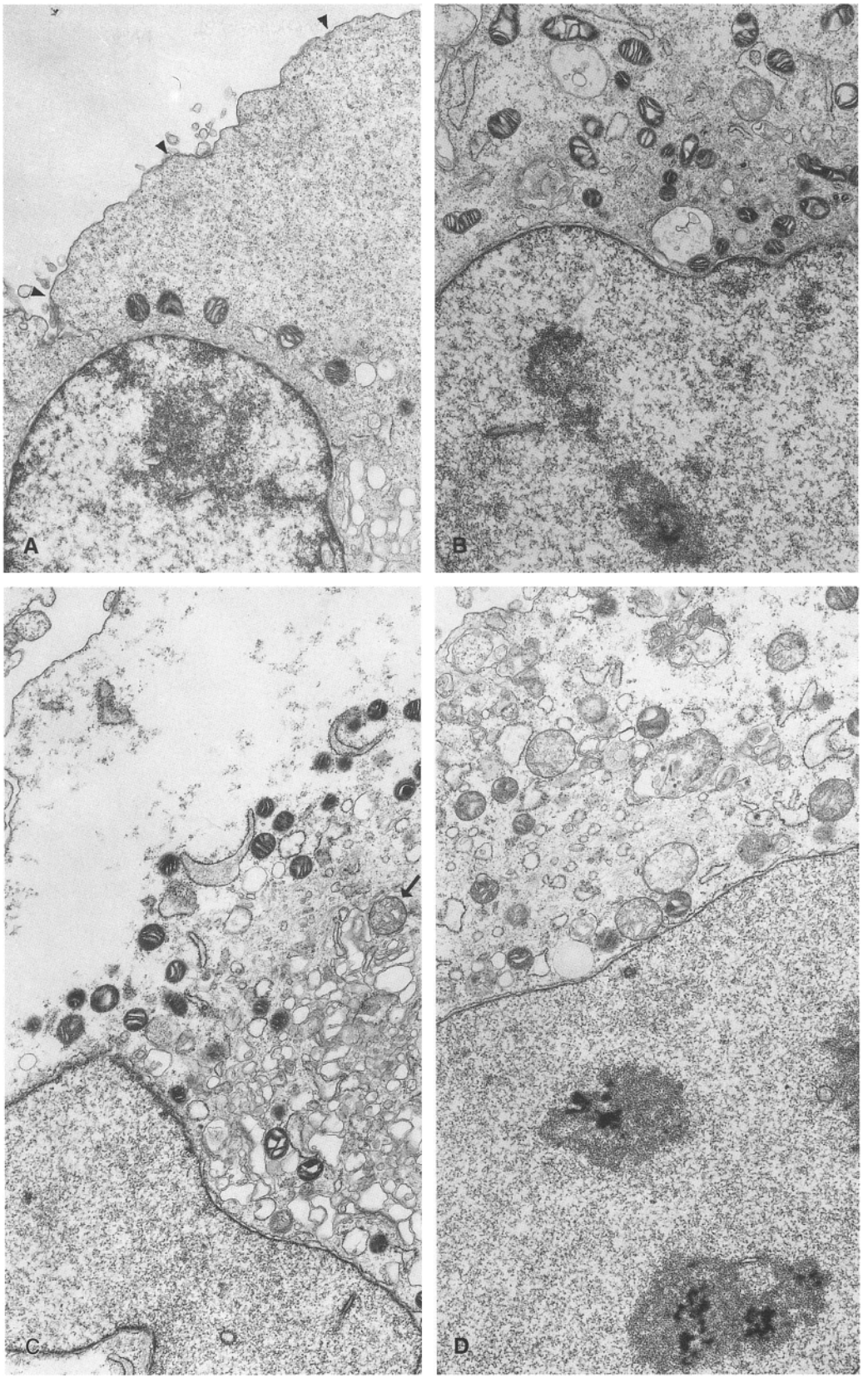

Fig. 5A Immediately after addition of C9 to cells bearing C5b–8 lesions at 0° C, the cytoplasmic organelles cluster around the nucleus and most of the microvilli are lost. The peripheral cytoplasm shows one early bleb *(arrows)*. The mitochondria are still in C-phase, but appear enlarged compared with the C5b–8 stage. (× 14,200) **B** At 1 min after C5b–9 lesion formation, at 37° C, the mitochondrial cristae swell further. The RER appears moderately dilated and the Golgi complex is disrupted. The nucleolus shows small electron-dense precipitates. (× 13,300) **C** At 3 min after C5b–9 lesion formation, at 37° C, most mitochondria are still in the C-phase, but some mitochondria are in the S-phase *(arrow)*. The outer cytoplasm is markedly extracted. The nuclear chromatin is dissolved except for a thin rim attached to the inner aspect of the nuclear envelope. (× 12,800) **D** At 5 min after C5b–9 lesion formation, at 37° C, almost all mitochondria are in the S-phase. The nucleoli show prominent globular or linear electron-dense formations. (× 13,300)

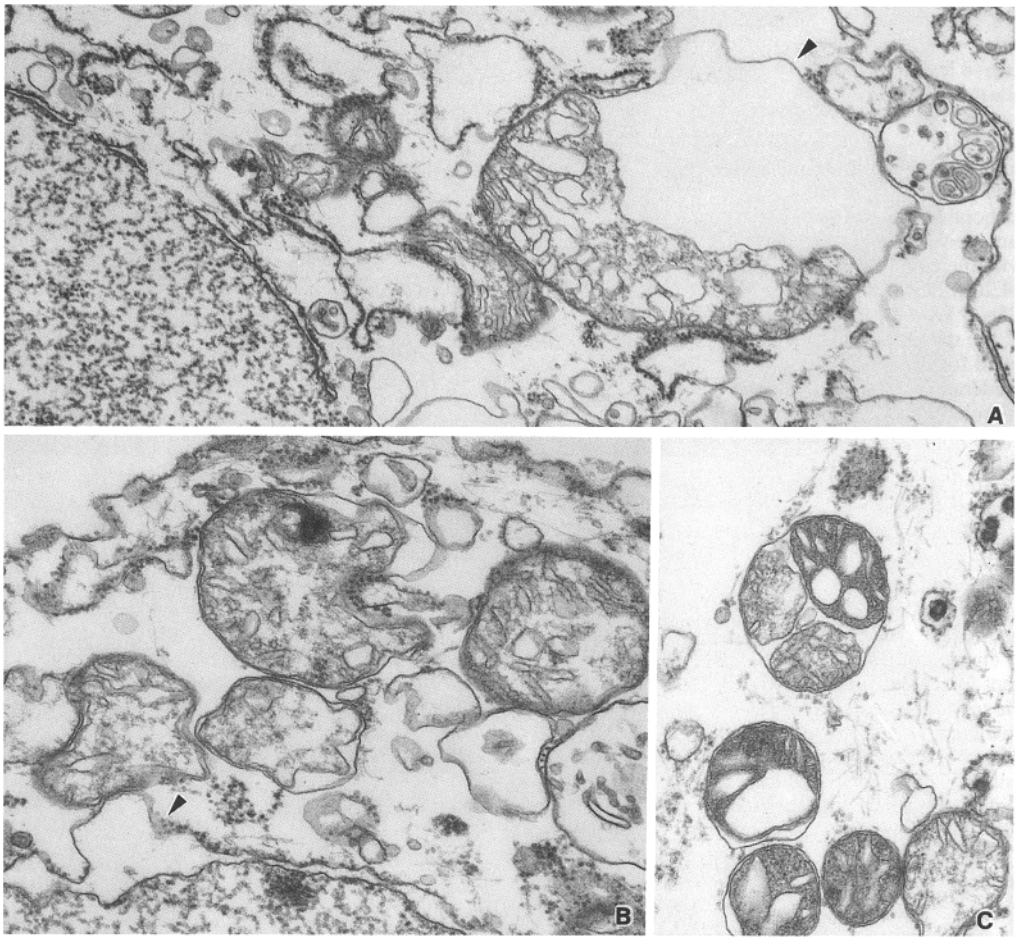

Fig. 6A At 15 min after C5b–9 lesion formation, at 37° C, the mitochondria are markedly swollen, in both matrical and cristal spaces, with blister formation in the latter *(arrow)*. (× 32,800) **B** At 15 min after C5b–9 formation, at 37° C, flocculent densities are seen within the mitochondrial matrix. The RER of the nuclear envelope appears dilated *(arrow)*. (× 34,800) **C** At 15 min after C5b–9 formation, at 37° C, occasional mitochondria show different segments showing concurrent C- and S-phase-type changes. (× 34,900)

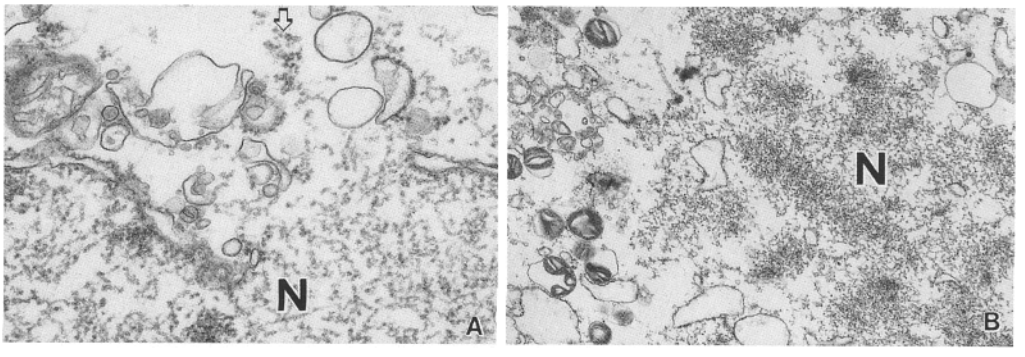

Fig. 7A At 15 min after C5b–9 formation, at 37° C, the nuclear envelope is markedly distended, with leakage of chromatin through disrupted nuclear pores into the cytoplasm *(arrow)*. *N* Nucleus. (× 32,000) **B** As soon as 5 min after C5b–9 formation, at 37° C, some cells show complete dissolution of the nuclear envelope. *N* Nucleus (× 11,200)

mations. The mitochondria remained condensed. The endoplasmic reticulum showed marked focal dilatation, whereas the still-recognizable Golgi complex showed some disorganization. The cytoplasm and nucleoplasm showed mild extraction.

At 37° C the plasma membrane progressively showed simplification, concomitant with the cell swelling (Fig. 5C–5D). Prominent cytoplasmic blebs were formed as little as 1 min after transfer to 37° C. The blebs were devoid of cytoskeletal elements. The latter appeared collapsed at the base of the bleb. The cell swelling was in many istances accompanied by breaks in continuity of the plasma membrane.

At 1 min after transfer to 37° C (Fig. 5B), the mitochondrial matrix remained condensed, but the cristae showed marked dilatation. At 3 min (Fig. 5C), most mitochondria still showed this morphology, whereas a minority appeared swollen (S).

At 5 min (Fig. 5D), most mitochondria showed the S-configuration, whereas at 15 min large dilatations of the outer mitochondrial space with occasional blister formation were noted (Fig. 6A). Flocculent densities within the matrical space were also present at that point (Fig. 6B). Also at that time point, some mitochondria displayed a hybrid pattern, i.e., one compartment was condensed whereas another was swollen (Fig. 6C).

The ER cisternae showed marked dilatation shortly (1 min) after transfer to 37° C (Fig. 5B). The dilatation involved the nuclear envelope extensively. With time progression, both the ER and the Golgi complex appeared as aggregates of non-oriented vesicles (Fig. 5C, D).

The cytosol showed progressive extraction (Fig. 5B–D), with almost total clearing in the peripheral portions (Fig. 5C). The cytoskeletal filaments, which were indistinct in untreated cells and in TAC9 cells at 0° C (Fig. 5A), became progressively discernible, along with the clustering of organelles around the nucleus (Fig. 5C, D).

The nuclei showed marked swelling shortly (1 min) after transfer to 37° C (Fig. 5B), becoming more rounded in shape – as opposed to the more ovoid shape of nuclei of untreated cells. This swelling was accompanied by dissolution of the heterochromatin (Fig. 5B–D), including the nucleolus-associated chromatin (Fig. 5B, D). The nucleoli themselves showed markedly electron-dense fibrillar deposits in their centers (Fig. 5B) becoming progressively more prominent (Fig. 5D), in keeping with segregation of the nucleolar components.

The nuclear envelope remained initially intact, despite the marked nuclear swelling. Focal dilatations of the nuclear envelope associated cisterna were, however, present. At 15 min, marked distention of the nuclear pores was noted with leakage of chromatin material into the cytoplasm (Fig. 7A). In few cells, the nuclear envelope disintegrated totally by 5 min, releasing the whole of the chromatin into the cytoplasm (Fig. 7B).

Discussion

The biochemical mechanisms involved in the complement-mediated cell death have not previously been clearly defined. In a previous paper, we have shown that osmotic protection fails to prevent cell death despite the lack of cell swelling, i.e., the kinetics of cell death were similar irrespective of cell volume changes (Kim et al. 1989). We further showed that the marked calcium influx occurring immediately after complement-mediated injury – as we and other investigators (Campbell et al. 1979, 1981; Seeger et al. 1986) have demonstrated – is directly associated with extinction of mitochondrial membrane potential and subsequent cell death (Papadimitriou et al. 1991b, c, 1994). We also showed that the cell ATP content falls precipitously in association to the mitochondrial failure, but also due to presumed increased consumption and the demonstrated adenine nucleotide leakage through the transmembrane complement channels (Papadimitriou et al. 1991a).

Thus, complement-mediated injury is characterized by: (a) immediate and massive cytosolic calcium ($[Ca^{2+}]_i$) increase; (b) leakage of ATP and its precursors through the transmembrane channels; and (c) disruption of the osmotic barrier of the cell membrane.

In this communication, we correlate the morphological changes of the cell and its organelles to the biochemical changes outlined above.

A striking finding observed in complement injury was the "ultracondensation" of mitochondria after C5b–8 formation. This change could be explained with reference to the "mechanochemical" theory (Hackenbrock 1966, 1968), which proposes that different states of respiration are associated with conformational changes of mitochondrial membrane proteins and associated active contraction of the inner membrane component, or the "osmotic" theory (Deamer et al. 1967), according to which the change is a result of ion movements through the mitochondrial membrane with accompanying movement of water.

In the former case, the normal mitochondria would contract as part of a physiological response to increase their respiration in order to cope with the osmotic load that results from sublytic complement injury such as occurs with C5b–8 channels (Fig. 4A). C5b–8 lesions possess channel properties corresponding to 0.4–3 nm diameter (Ramm et al. 1982). We have also shown previously that minor adenine nucleotide leakage can occur through these lesions (Papadimitriou et al. 1991a), a phenomenon that we were again able to confirm in the current studies. Significantly, in this situation the mitochondria retain their membrane potential and the cell ATP levels remain stable (Papadimitriou et al. 1991a).

In the latter case, the injured mitochondria would lose excessive K^+ – a major mitochondrial ion – and, therefore, H_2O. In cell injury in general, the mitochondria have less ability to maintain their bound K^+ (Lehninger et al. 1967). In the case of complement injury, the decreased cytoplasmic K^+, as a result of K^+ efflux through the membrane channels (Ramm et al. 1982), could enhance the mitochondrial K^+ loss and thus lead to further matrical shrinkage. This hypothesis is plausible during the initial phase after C5b–9 lesion formation, when the mitochondria appear morphologically condensed (Fig. 5A–C) but have lost their membrane potential and the cell ATP levels decrease precipitously (Papadimitriou et al. 1991a).

Otherwise, the series of mitochondrial changes appeared to recapitulate the pattern observed with various other forms of cell injury, including interference with membrane function, e.g., binding of -SH groups with PCMBS (Laiho and Trump 1975). This pattern includes progression from the orthodox to the condensed and finally to the swollen morphology. However, the kinetics of these changes after complement membrane attack were faster than with other forms of cell injury, the whole range being completed within less than 15 min. It is most probable that the changes in $[Ca^{2+}]_i$, being more dramatic in the case of complement injury than with other injurious insults, account for these phenomena. The mitochondria represent physiologically a major locus for $[Ca^{2+}]_i$ buffering (for review see Lehninger 1982). In the case of complement injury, the excessive load of Ca^{2+} that accumulates in the mitochondria would potentially lead to both abolition of their energy production capacity – by neutralizing the transmembrane potential, as previously observed (Papadimitriou et al. 1991a) – and also to

their autolysis through activation of the Ca^{2+}-dependent phsopholipase (Waite et al. 1969). The leakage of ATP, ADP and AMP (Papadimitriou et al. 1991a) could contribute to that effect, through decrease of the intramitochondrial ATP. The latter has been suggested to act as an inhibitor to the phospholipase activity (Parce et al. 1978). A considerable amount of information has recently also been gathered on the mitochondrial "permeability transition," an initially reversible Ca^{2+}-induced increase in the inner membrane permeability (for review see Gunter and Pfeiffer 1990). ADP is a significant inhibitor of the permeability transition, and its loss to the medium through the C5b–9 channels (Papadimitriou et al. 1991a) could lead – in synergy with the massive Ca^{2+} influx – to perpetuation of that condition. Thus, we postulate that in complement injury the constellation of changes leads to a vicious cycle resulting in unbuffered high $[Ca^{2+}]_i$.

The nuclear changes in complement-mediated cell injury are also noteworthy. The disappearance of heterochromatin could theoretically represent DNA hydrolysis by a Ca^{2+}-activated endogenous endonuclease. The latter phenomenon has been claimed not to occur after complement injury – as opposed to lymphocyte-mediated injury (Duke et al. 1983). Thus, the cell-mediated cytotoxicity has been considered as a case of "apoptosis," which is characterized by internucleosomal DNA degradation induced by an endonuclease (for review see Schwartzman and Cidlowski 1993), whereas complement-mediated cell death has been considered as "necrosis." However, other investigators have observed some DNA hydrolysis after complement injury, which they also attributed to activation of an endonuclease (Shipley et al. 1971).

On the other hand, the disappearance of heterochromatin could be related to loss of volume control of the nucleus, not necessarily with concomitant DNA digestion. Significantly with C5b–9 injury we have indication of nuclear envelope damage, as propidium iodide staining of the nuclei is observed after only 5 min, i.e., very early (Papadimitriou et al. 1991a).

Thus, in general, the complement-mediated injury appears to lead to the opposite pattern of nuclear changes to typical apoptosis: heterochromatin disappearance rather than condensation; nuclear swelling with chromatin leakage to the cytoplasm (Fig. 7A) rather than shrinkage; loss of the ability to exclude dyes such as trypan blue or propidium iodide rather than preservation of that ability.

However, the one nuclear change that appears to be similar in both apoptosis and C5b–9 injury is that in the nucleoli. The latter show segregation of their components (Fig. 5D) in both cases. The fact that these nucleolar changes appeared also in cells bearing C5b–8 lesions, which were not swollen and were not yet dead (i.e., no LDH release was observed) indicates that milder forms of complement injury could theoretically lead to apoptosis in appropriate circumstances. These milder forms of complement attack could be more relevant in vivo, where homologous restriction (for review see Papadimitriou et al. 1990) would play a moderating role.

In summary, the morphological changes in complement-mediated cell injury appear to overlap with other known forms of cell injury – although the sequence is much more rapid – but also to present some particular features related to the nature of this form of insult. Specifically, the immediate and massive increase in $[Ca^{2+}]_i$ (Papadimitriou et al. 1991b) is most probably responsible for the rapid mitochondrial destruction and for the activation of other autolytic enzymes located in the plasma membrane, cytoplasm, nucleus and other locations (for review see Trump and Berezesky 1992), leading to the morphological changes described in this communication.

Acknowledgements Supported by NIH AI 19622, NS15662, DK15440, Navy N00014-88-K-0427, and a grant to J.P. from ACS MD Div.

References

Campbell AK, Daw RA, Luzio JP (1979) Rapid increase in intracellular free CA^{2+} induced by antibody plus complement. FEBS Lett 107:55–60

Campbell AK, Daw RA, Hallett MB, Luzio JP (1981) Direct measurement of the increase in intracellular free calcium ion concentration in response to the action of complement. Biochem J 194:551–560

Carney DF, Koski CL, Shin ML (1985) Elimination of terminal complement intermediates from the plasma membrane of nucleated cells: the rate of disappearance differs from cells carrying C5b–7 or C5b–8 with a limited number of C5b–9. J Immunol 134:1804–1809

Deamer DW, Utsumi K, Packer L (1967) Oscillatory states of mitochondria. III. Ultrastructure of trapped conformational states. Arch Biochem Biophys 121:641–651

Duke RC, Chervenak R, Cohen JJ (1983) Endogenous endonuclease-induced DNA fragmentation: an early event in cell-mediated cytolysis. Proc Natl Acad Sci USA 80:6361–6365

Gunter TE, Pfeiffer DR (1990) Mechanisms by which mitochondria transport calcium. Am J Physiol 258 [Cell Physiol 27]:C755–C786

Hackenbrock CR (1966) Ultrastructural basis for metabolically linked mechanical activity in mitochondria. I. Reversible ultrastructural changes with change in metabolic steady state in isolated liver mitochondria. J Cell Biol 30:269–297

Hackenbrock CR (1968) Ultrastructural basis for metabolically linked mechanical activity in mitochondria. II. Electron transport-linked ultrastructural transformations in mitochondria. J Cell Biol 37:345–369

Kabat EA, Mayer MM (1961) Experimental immunochemistry. Thomas, Springfield, Ill

Kim SH, Carney DF, Papadimitriou JC, Shin ML (1989) Effect of osmotic protection on nucleated cell killing by C5b–9: cell death is not affected by the prevention of cell swelling. Mol Immunol 26:323–331

Koski CL, Ramm LE, Hammer CH, Mayer MM, Shin ML (1983) Cytolysis of nucleated cells by complement: cell death displays multi-hit characteristics. Proc Natl Acad Sci USA 80:3816–3820

Laiho KU, Trump BF (1975) Studies of the pathogenesis of cell injury: effects of inhibitors of metabolism and membrane function on the mitochondria of Ehrlich ascites tumor cells. Lab Invest 32:163–182

Laiho KV, Shelburne JD, Trump BF (1971) Observations on cell volume, ultrastructure, mitochondrial conformation and vital-dye uptake in Ehrlich ascites tumor cells. Effects of inhibiting energy production and function of the plasma membrane. Am J Pathol 65:203–217

Lehninger AL (1982) Principles of biochemistry. Worth Publishers, New York, pp 482–483

Lehninger AL, Carafoli E, Rossi CS (1967) Energy-linked ion movements in mitochondrial systems. Adv Enzymol 29:259–320

Luft JH (1961) Improvements in epoxy resin embedding methods. J Biophys Biochem Cytol 9:409–414

Marzella L, Trump BF (1992) Pathology of the cell: ultrastructural features. In: Papadimitriou JM, Henderson DW, Spagnolo DV (eds) Diagnostic ultrastructure of non-neoplastic diseases. Churchill Livingstone, Edinburgh, pp 46–83

Papadimitriou JC, Shin ML, Hänsch GM (1990) Mechanisms of complement-mediated membrane damage. In: Mergner WJ, Jones RT, Trump BF (eds) Cell death: mechanisms of acute and lethal cell injury, vol 1, chap 3. Field & Wood, Philadelphia, pp 67–85

Papadimitriou JC, Ramm LE, Drachenberg CB, Trump BF, Shin ML (1991a) Quantitative analysis of adenine nucleotides during the prelytic phase of cell death mediated by C5b–9. J Immunol 147:212–217

Papadimitriou JC, Phelps PC, Ramm LE, Drachenberg CB, Shin ML, Trump BF (1991b) Increased $[Ca^{2+}]_i$ followed by failure of energy metabolism mediates Complement (C)-induced cell death in Ehrlich Ascites tumor cells (EATC) (abstract). (75th Annual Meeting, Federation of American Societies for Experimental Biology, Atlanta, Ga, 1991). FASEB J 5:A1670

Papadimitriou JC, Phelps PC, Ramm LE, Drachenberg CB, Trump BF, Shin ML (1991c) Loss of mitochondrial membrane potential and adenine nucleotide depletion during prelytic phase of C5b–9 attack on nucleated cell (abstract). (XIV International Complement Workshop, Cambridge, UK, 1991) Complement Inflamm 8:205

Papadimitriou JC, Carney DF, Shin ML (1991d) Inhibitors of membrane lipid metabolism enhance complement-mediated nucleated cell killing through distinct mechanisms. Mol Immunol 28:803–809

Papadimitriou JC, Phelps PC, Shin ML, Trump BF (1994) Effects of Ca^{2+} deregulation on mitochondrial membrane potential and cell viability in nucleated cells following lytic complement attack. Cell Calcium 15:217–227

Parce JW, Cunningham C, Waite M (1978) Mitochondrial phospholipase A2 activity and mitochondrial aging. Biochemistry 17:1634–1639

Ramm LE, Whitlow MB, Mayer MM (1982) Size of the transmembrane channels produced by complement proteins C5b–8. J Immunol 129:1143–1146

Saladino AJ, Bentley PJ, Trump BF (1969) Ion movements in cell injury. Effect of amphotericin B on the ultrastructure and function of the epithelial cell of the toad bladder. Am J Pathol 54:421–466

Schwartzman RA, Cidlowski JA (1993) Apoptosis: the biochemistry and molecular biology of programmed cell death. Endocrine Rev 14:133–151

Seeger W, Suttorp N, Helwig A, Bhakdi S (1986) Noncytolytic terminal complement complexes may serve as calcium gates to elicit leukotriene B4 generation in human polymorphonuclear leukocytes. J Immunol 137:1286–1293

Shipley WU, Baker AR, Colten HR (1971) DNA degradation in mammalian cells following complement-mediated cytolysis. J Immunol 106:576–579

Thore A (1979) Technical aspects of the bioluminescent firefly luciferase assay for ATP. Sci Tools 26:30–34

Trump BF, Berezesky IK (1992) The role cytosolic Ca^{2+} in cell injury, necrosis and apoptosis. Curr Opin Cell Biol 4:227–232

Trump BF, McDowell EM, Arstila AU (1980) Cellular reaction to injury. In: Hill RB Jr, LaVia MF (eds) Principles of pathobiology, 3rd edn. Oxford University Press, New York, p 20

Venable JH, Coggeshall R (1965) A simplified lead citrate stain for use in electron microscopy. J Cell Biol 25:407–408

Waite M, van Deenen LLM, Ruigrok TJC, Elbers PF (1969) Relation of mitochondrial phospholipase A activity to mitochondrial swelling. J Lipid Res 10:599–608

Watson ML (1958) Staining tissue sections for electron microscopy with heavy metals. J Biophys Biochem Cytol 4:475–478